JOURNAL OF
ENVIRONMENTAL HYDROLOGY
The Electronic Journal of the International Association for Environmental Hydrology
On the World Wide Web at http://www.hydroweb.com
VOLUME 8 2000

CHANGES OF BED TOPOGRAPHY IN MEANDERING RIVERS AT A NECK CUTOFF INTERSECTION

Y. R. Fares
Department of Civil Engineering
University of Surrey
Guildford, Surrey
United Kingdom

On the basis of a field survey on bottom topography changes in the meandering river Allan Water at the cutoff (lateral overflow) section, a detailed study of velocities and boundary shear stresses in an idealized rigid bed model was undertaken. The characteristics of curved channel flows, i.e. secondary circulation and superelevation at the water surface, have been included in the formulation. The effect of lateral overflow on the curved flow is formulated by a spatially varied flow equation with decreasing discharge. The analysis of results has shown that continual reductions in velocities and shear stresses occurred in the channel at the lateral overflow region. Maximum reduction of velocities and shear stresses was 18 percent and 37 percent for cases of low lateral overflows, and 58 percent and 82 percent for cases of high side overflows respectively. These reductions were attributed to the development of stagnation and separation zones at the intersection associated with strong lateral outward currents. Finally, an explanation is provided for the marked bed topography changes in the Allan Water situation. The changes in shear stress field are found to be responsible for the initiation of a longitudinal bar in the middle of the channel and a deep scour hole close to the outer bank.

INTRODUCTION

Cutoff channels, as natural flood relief channels, are developed as the river adjusts to its course during high flood periods. Along a meandering river, zones of riffles and pools are continually formed as a result of the helical motion induced in the flow by channel curvature. Neck cutoff in a meandering river develops from the continuous redistribution of the bed topography due to effects of helical flow on sediment motion (Allen, 1965, Gagliano and Howard, 1983, Klaassen and van Zanten, 1989). As part of a study of flow mechanisms in meandering rivers, a field study was carried out on a meander loop/neck cutoff intersection at Allan Water, Perthshire, Scotland, as shown in Figure 1 (Herbertson and Fares, 1991). At the cutoff section of the river, Allan Water is 15 m wide, drains a catchment area of 210 km^2, and has an average annual flow of 6 m^3/s. The cutoff channel is also about 15 m wide, has a length of about 20 m and has a bed level approximately 1m above the river bed level (see Plate 1).

As a result of partial cutoff at the neck of this meander loop, marked changes in the bed topography of the river had occurred. These marked changes were found to vary considerably from that usually found in a meandering river. The traditional riffle/pool bed profile was completely destroyed, but the following features were observed (Figures 1 and 2):

(i) Development of a longitudinal bar at a distance of about 40 percent of the channel width from the front of the cutoff,

(ii) Formation of a deep scour hole at the downstream section of the river just beyond the cutoff intersection; and

(iii) Migration of the thalweg towards the inside of the river.

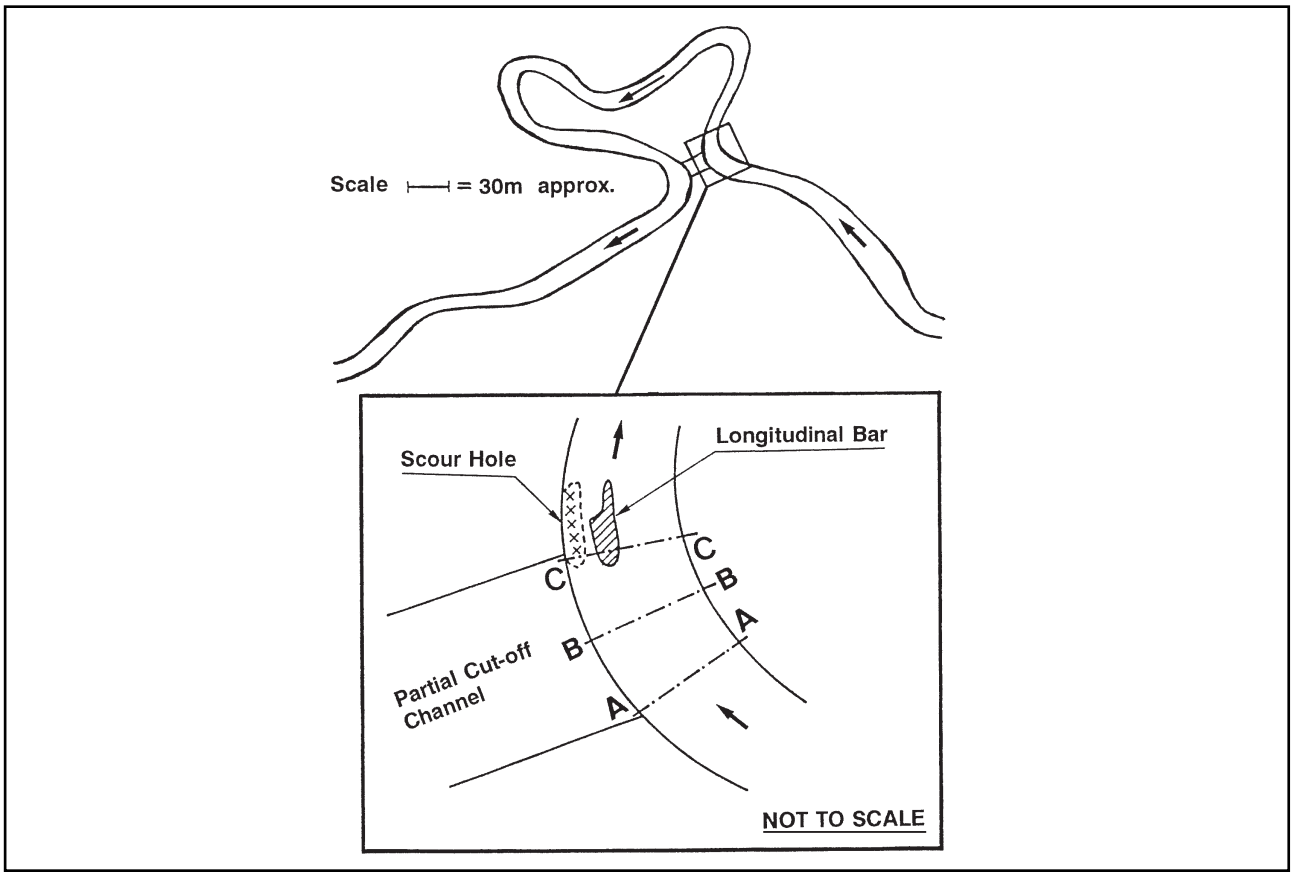

Figure 1. Cutoff section of meander loop at Allan Water.

Plate 1. Allan Water configuration at the cutoff section.

In order to understand the mechanisms associated with the complex features developed at the cutoff section of the river, numerical and experimental studies into the flow behavior in an idealized rigid-bed model situation were undertaken (Fares et al., 1992, Fares and Herbertson, 1993, Fares

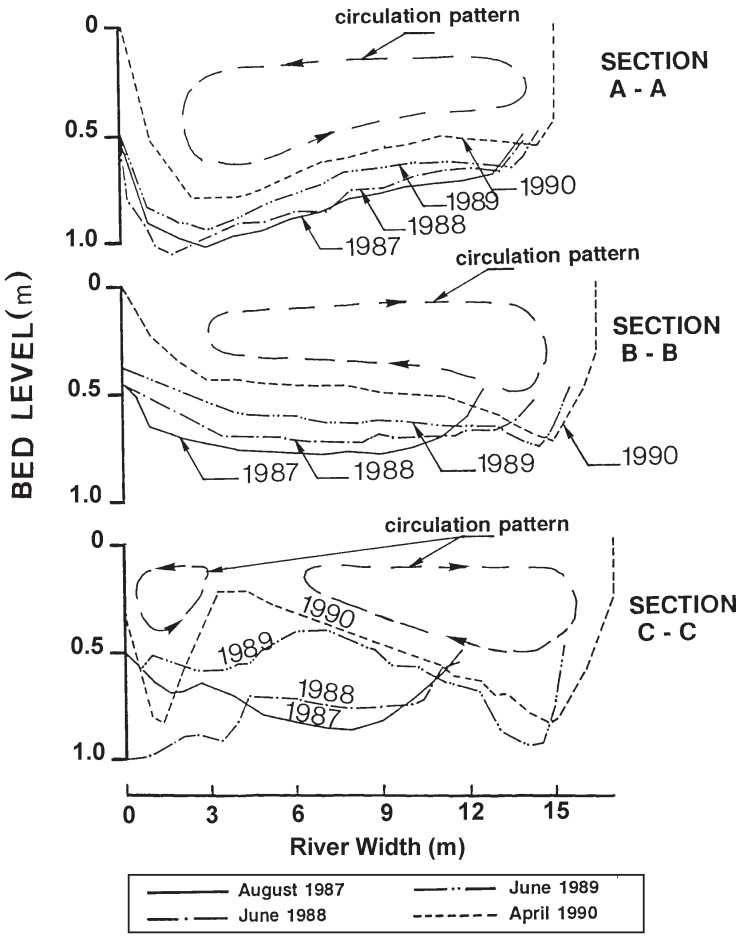

Figure 2. Bed topography profiles in Allan Water at cutoff section.

1995). On the basis of correlating the preliminary experimental findings from the idealized flow model with the features observed in the bed topography of the river, it was found that the change of the cell structure of the secondary flow is the main cause for such modifications (Herbertson, Fares, 1991). The observed cell structure change was developed from the classic "one-cell" secondary flow type to a "two-cell" type rotating in an opposite sense, one large cell between the bar and the inner bank and a smaller cell between the bar and the outer bank (Figure 2, section C-C). This two-cell type of circulation in front of the cutoff was responsible for the deposition of the loose material of the channel and hence, for the initiation of the longitudinal bar in the middle of the river cross section. Similarly, the formation of the deep scour hole downstream of the cutoff section and the inward migration of the thalweg were attributed to the two-cell secondary flow pattern. This pattern produced erosion on both banks of the meander, hence enhancing the process of scouring on the outside bank as well as causing inward shifting (or migration) of the thalweg.

The paper reports the development of a computational model aiming at quantifying the changes occurring to the curved channel flow features as a result of a cutoff channel intersection, simulated by a lateral overflow. The analytical formulation of the problem and the computational algorithm adopted in the solution are described. Particular attention is given to the changes in the velocity and boundary shear stress fields of the curved flow at the cutoff intersection region.

FORMULATION OF THE PROBLEM

The combination of a 2-D curved flow model and a spatially varied flow equation represents the core of the mathematical formulation of the problem. The formulation is divided into two main stages. The analytical formulation pertaining to flow in a gently curved channel will be considered first. This will be followed, in the second stage, by simulating the effects of the cutoff channel intersection on the curved flow characteristics. Entry to the cutoff channel is controlled by, and simulated as, a side overflow of arbitrary crest level. Details of the numerical scheme and the procedure adopted in the solution of the horizontal problem of the curved flow will be presented.

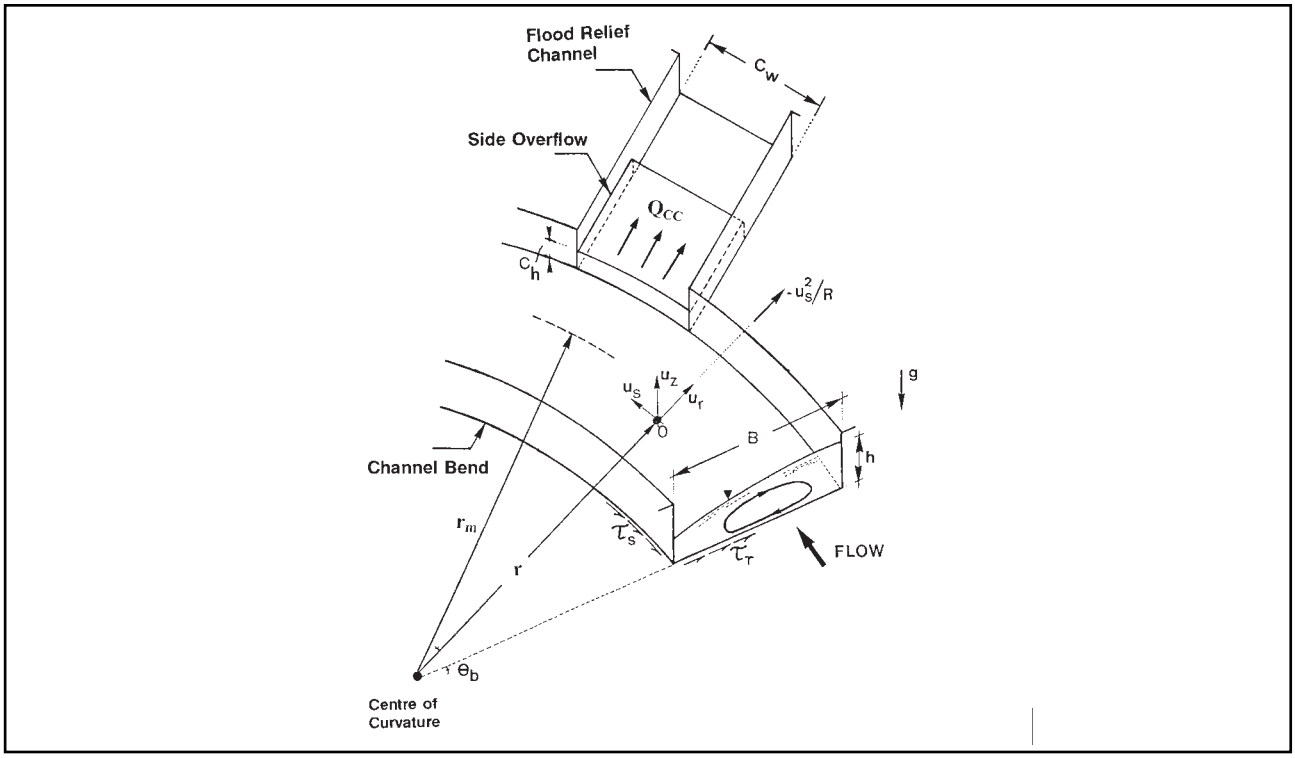

Figure 3. Idealized rigid bed model of curved channel with side overflow.

Formulation of 2-D curved channel flow

In curved channels, the flow field is three-dimensional. However, as the depth of water in rivers is normally much smaller than their widths and lengths, 2-D models are most conducive to the study of the flow field in meandering channels. The flow field is normally resolved into streamwise and crosswise components, because of the effects of water surface superelevation, secondary flow and boundary resistance. In general, uncertainties in computations are found to vary with flow depth but to be highly influenced by uncertainties in secondary flow (De Vriend, 1981, Siegenthaler and Shen, 1983, Johannesson and Parker, 1989). Figure 3 shows the cylindrical coordinates of the system (r, s, z) in the radial, longitudinal and vertical directions from an arbitrary origin at the bottom of the channel. In the formulation, the shear stress field is calculated from the depth-averaged velocities $u_m(r,s)$. By considering the momentum equation in the s-direction, the balance of depth-averaged forces applied to an elementary area ($dr.ds$) is given by (Fares et al., 1992, Fares, 1995):

$$\frac{\partial \Phi_1}{\partial s} + \frac{1}{r^2}\frac{\partial}{\partial r}\left(r^2 \Phi_2\right) = g S_s h - u_*^2 \tag{1}$$

where (∂r , ∂s) = gradient operators in the r- and s-directions respectively; h = local flow depth; r = local bend radius; S_s = streamwise flow surface slope; $u_* = (\tau_s/\rho)^{1/2}$ = shear velocity, with τ_s = streamwise component of the shear stress field (τ_r , τ_s), and ρ = flow density; and g = acceleration due to gravity. In Equation (1) the convective transport of the streamwise momentum by the cross (secondary) flow is essential for the development of the depth-averaged velocity pattern, and hence the shear stress field. The functions $\Phi_1(r,s)$ and $\Phi_2(r,s)$ are given by:

$$\Phi_1 = \beta h u_m^2 \quad \text{and} \quad \Phi_2 = \alpha \frac{h^2}{r_m} u_m^2 \tag{2}$$

where $\Phi_1(r,s)$ and $\Phi_2(r,s)$ represent the contribution of the streamwise and crosswise momentum to flow motion respectively. The coefficients β and α are the corresponding main and secondary flow convection factors for $\Phi_1(r,s)$ and $\Phi_2(r,s)$ respectively. The ratio of the secondary flow convection to that in the main direction can be obtained by dividing Φ_2(r,s) by $\Phi_1(r,s)$ as:

$$\frac{\Phi_2}{\Phi_1} = \frac{\alpha}{\beta}\left(\frac{h}{r_m}\right) = \frac{\alpha}{\beta}\left(\frac{h}{B}\right)\left(\frac{B}{r_m}\right) \tag{3}$$

That is the secondary flow convection ratio F_2/F_1, decreases with increasing aspect ratio B/h and bend tightness r_m/B, where r_m = bend mid radius and B = channel width. Therefore the shallower the flow and less tight the bend, the less the contribution is of the secondary flow for a given channel roughness. As expected, this indicates a greater dispersion of flow momentum in the crosswise direction for roughened channels and strongly curved flows (Kalkwijk and De Vriend, 1980). From the solution of Equation (1), the shear stress field $\tau_0(r,s) = (\tau_r , \tau_s)$ can be determined from the convection functions $\Phi_1(r,s)$ and $\Phi_2(r,s)$ which, in turn, are dependent on the velocity field $u_m(r,s)$. The streamwise component of shear stress $\tau_s(r,s)$ being dependent solely on the streamwise convection was calculated from a standard resistance equation, e.g. Chezy's equation, as:

$$u_* = \sqrt{\frac{\tau_s}{\rho}} = u_m \frac{\sqrt{g}}{C} \tag{4}$$

where C = Chezy coefficient of boundary roughness. The crosswise stress component $\tau_r(r,s)$ was calculated from (Bouwmeester, 1972, Fares 1995):

$$\frac{\tau_r}{\rho} = 2\frac{h}{r}u_m^2\zeta^2(1-\zeta) \quad \text{with} \quad \zeta = \sqrt{\frac{g}{\kappa C}} \tag{5}$$

where κ = von-Karman constant. In Equation (5), $\tau_r(r,s)$ depends strongly on u_m and the h/r ratio. For cases of curved flows of same velocities and roughness coefficients, the transverse stress component $\tau_r(r,s)$ increases with flow depth $h(r,s)$ and with decreasing bend tightness r_m/B. It should be stated that Equation (5) is only applicable within 80-90 percent of the river cross section, away from the bank regions. The effects of boundary layer regions along banks in meandering channels are generally neglected for flow cases of $B/h \geq 8$ and $r_m/B \geq 3$ (e.g. Zimmermann and Kennedy (1978), Chen and Shen (1983)). The relationship between the flow convection ratio Φ_2/Φ_1 and the shear stress ratio τ_r/τ_s can consequently be determined by:

$$\frac{\Phi_2}{\Phi_1} = \frac{\kappa^2}{2(\zeta-1)}\left(\frac{\alpha}{\beta}\right)\left[\frac{\tau_r}{\tau_s}\right] \tag{6}$$

From Equation (6) it can be deduced that the transverse shear stress increases by increasing both bed roughness and the intensity of the transverse flow in the motion, as expressed by the secondary flow convection factor α/β. Once a solution for the horizontal problem (i.e. for $u_m(r,s)$ and $h(r,s)$) is obtained, the boundary shear stress field $\tau_0(r,s)$ can be determined.

Formulation of quasi 2-D flow at overflow region

For the case of combined curved and active lateral flows, the discharge dQ_{cc} over a step length dC_w across the side overflow can be calculated from:

$$\frac{dQ_{cc}}{dC_w} = A_w D_f (h - C_h)^{3/2} \tag{7}$$

where A_w = a weir coefficient including velocity and discharge coefficients; D_f = coefficient for simulating the drowning condition over the weir (≥ 1); C_h = weir crest height; and $h(r,s)$ = water head in the bend channel. The streamwise variation of bend flow at the intersection can be simulated by the spatially varied flow equation, with decreasing discharge, pertaining along the crest width of the overflow, i.e.

$$\frac{dh}{dC_w} = \frac{S_0 - S_f - \left(\frac{\lambda}{A^2}\right)\frac{dQ_{cc}}{dC_w}\left[uA + dQ_{cc}\right]}{1-\beta\left(F_r^2 + \Delta F_r^2\right)} \tag{8}$$

with

$$\frac{\Delta F_r^2}{F_r^2} = \frac{Q_{cc}}{Q} \quad , \quad F_r = \frac{u}{\sqrt{gh}} \quad , \quad \lambda = \frac{2\beta - 1}{g} \tag{9}$$

where S_0 = bed slope of the river; S_f = friction slope; u = sectional velocity of bend flow; F_r = Froude number; and A = curved flow area (= Bh). Equation (8) is the basic equation for modeling the lateral

overflow effects on the flow in the main channel. However, since the main difference between flows in straight and curved channels is the effects of superelevation and secondary circulation, direct application of Equation (8) would certainly lead to unrealistic solutions. Hence the manner in which it is applied has to be modified to include these effects. As will be discussed in the following section, this was accomplished by dividing the bend cross section into a series of concentric strips of equal width, each of which has a certain (mean) depth and a certain (mean) velocity. As such, Equation (8) is applied to each concentric strip separately. The advantage of using this approach is that each concentric strip contributes to the overflow according to its mean water depth. The contribution increases as water elevation increases and hence, strips closest to the outer bank of the channel contribute most to the side overflow. The accuracy of the predictions depends mainly on the degree of channel curvature r_m/B and the aspect ratio of the flow B/h. The shallower and less curved the bend, the more realistic are the predictions.

CALCULATION PROCEDURE

There are two separate stages in the calculation procedure of the problem. The first stage deals with the calculation of the flow pattern in a curved channel without lateral (cutoff) overflows, which represents the "bend-only" situation. In the second stage, the calculation of the curved flow pattern at the cutoff (overflow) intersection is determined.

For the "bend-only" situation, Equation (1) can be expressed in a finite difference form as:

$$\frac{\Delta u_m}{\Delta s} = \frac{-1}{r_i}\left[\frac{\Delta(hu_m)}{\Delta r} + \frac{h_i^j}{2r_i}u_{m_i^j}\right] + \frac{(S_s)_i^j}{2}\left[\frac{g}{\beta u_{m_i^j}} - \left(\frac{u_m}{h}\right)_i^j\right] - \frac{g}{2\beta C^2}\left(\frac{u_m}{h}\right)_i^j \tag{10}$$

where

$$\Delta r = r_{i+1} - r_i \quad , \quad \Delta s = r_i \Delta\theta_b \quad , \quad \Delta\theta = \theta_b^{j+1} - \theta_b^j \tag{11}$$

$$\Delta u_m = u_{m_i}^{j+1} - u_{m_i}^j \tag{12}$$

$$\Delta(hu_m) = (hu_m)_i^{j+1} - (hu_m)_i^j \tag{13}$$

$$(S_s)_i^j \frac{\left(u_m^2\right)_i^j}{gC^2 h_i^j} \tag{14}$$

where $[i,j]$ = indices for r- and s- directions respectively; θ_b = local angle along the curved channel.

In the first stage of calculations, the bend channel is divided into a concentric mesh (see Figure 4) where at each grid point $u_m[i,j]$ is computed. The computations start at the inner bank and proceed in radial increments Δr to the outer bank. Then the computations proceed longitudinally in steps of Δs. The step size was carefully selected in order to preserve the consistency and accuracy requirements of the computations. The initial value of $S_S[i,j]$ at the curved channel entrance (i.e. at $\theta_b = 0^o$) was assumed to match that of the uniform flow at the upstream reach of the curve. Subsequent values of $S_S[i,j]$ were calculated from Equation (14). For the case of combined channel and overflow intersection, the dynamic equations, Equations (7) to (9), can be expressed as:

$$\left(Q_{cc}\right)_i^{\ell+1} = \left(Q_{cc}\right)_i^{\ell} + A_w D_f \left(h_i^{\ell} - C_h\right)^{3/2} \Delta C_w^{\ell} \tag{15}$$

$$\frac{\Delta h}{\Delta Cw} = S_0 - \left(S_f\right)_i^{\ell} - \frac{\lambda}{\left(A^2\right)_i^{\ell}} \left[A_i^{\ell} u_{m_i^{\ell}} + \Delta Q_{cc}\right] / \left[1 - \beta \left\{\left(F_r^2\right)_i^{\ell} + \left(\Delta F_r^2\right)_i^{\ell}\right\}\right] \tag{16}$$

$$\Delta Q_{cc} = \left(Q_{cc}\right)_i^{\ell+1} - \left(Q_{cc}\right)_i^{\ell} \quad , \quad A_i^{\ell} = u_{m_i^{\ell}} h_i^{\ell} \quad , \quad \Delta h = h_i^{\ell+1} - h_i^{\ell} \tag{17}$$

where [*i*,*l*] = indices for *r*- and *s*- directions at the side overflow section of the channel.

In the second stage of calculations, the channel cross section at the overflow region is divided into a series of concentric strips of equal width (see Figure 4). At each node [*i*,l], depth and velocity values were interpolated and assigned to each concentric strip. The initial values of depth and velocity at each grid node of the intersection region were fed from the output of the bend model, Equations (10) to (14). The depth and velocity profiles at the side overflow were obtained by the numerical integration of Equations (15) and (16) simultaneously (Price, 1977, Chapra and Canale, 1985). For cases of subcritical flow conditions, the computations start at the downstream end of the intersection and proceed towards the upstream end. However, in evaluating $h\,[i,\ell]$ and $u_m[i,\ell]$ of the approach flow, the calculations had to be carried out in the downstream direction. Hence an assumption for the

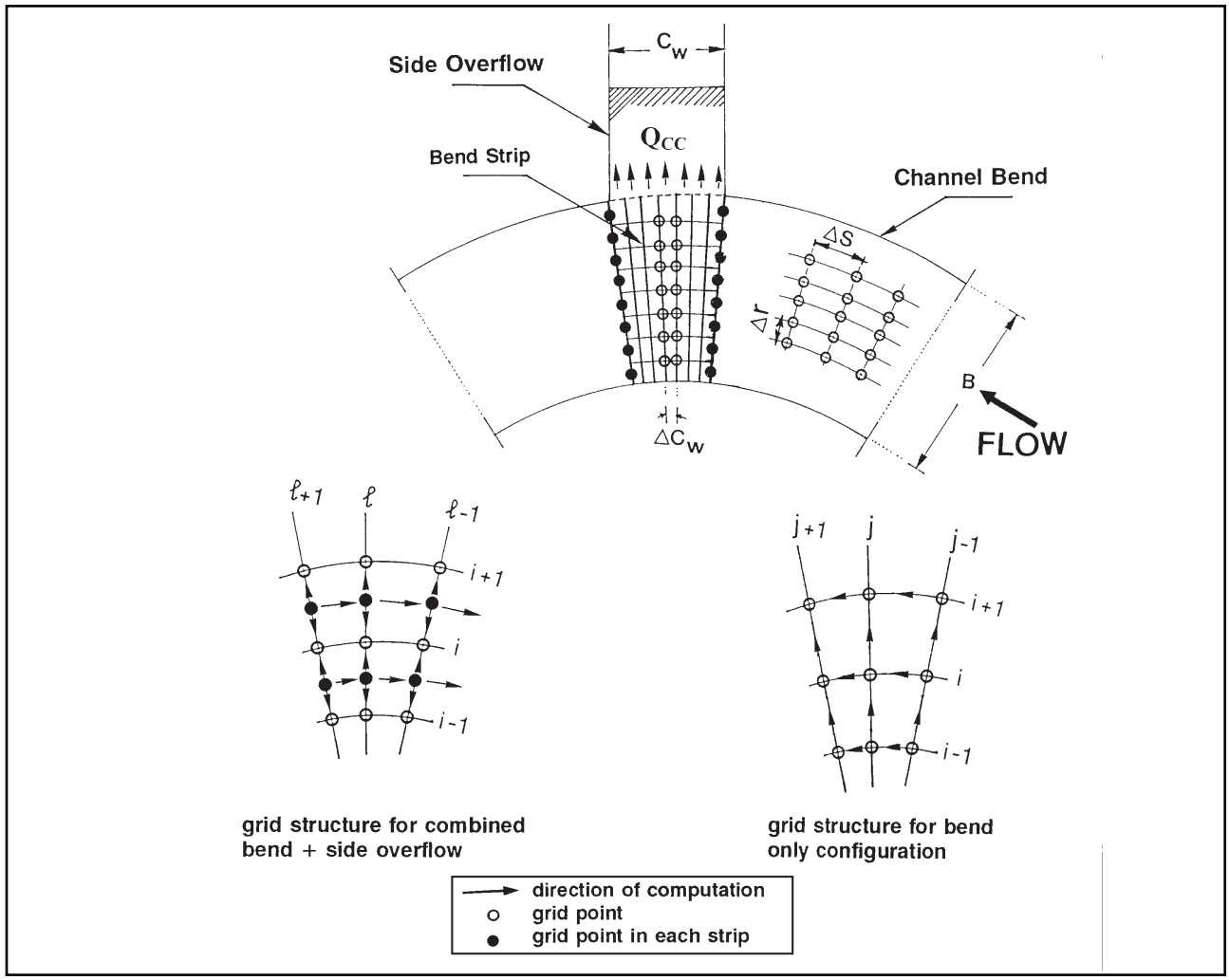

Figure 4. Grid structure used in model computations.

curved flow at the intersection was necessary for the computations to proceed from the downstream end towards the upstream end. The assumption used was that the specific energy in each strip of the channel was kept constant. This allowed $h\,[i,\ell]$ and $u_m\,[i,\ell]$ to be calculated at the downstream end, from which the computations start. It should be emphasized that this assumption does not imply a constant energy across the channel width, since energy variations are implicitly introduced through $h[i,\ell]$ and $u_m\,[i,\ell]$. This assumption, however, has been previously employed by Ranga Raju et al. (1979) and Uyumaz and Muslu (1985), and was found to produce realistic results. Details of the FORTRAN program (CURCLOV code) that have been developed for carrying out the necessary computations are given in Fares (1994).

CHANGES IN CURVED FLOW MECHANISMS

For the purposes of verifying the computational model, data were used from an experimental study on a 60° rigid bed curved channel with a side overflow (Fares and Herbertson 1993). The side overflow is placed at the outer bank between angle θ_b = 25° and 35° in order to allow significant development of superelevation and secondary circulation in the flow. The width ratio between the overflow and channel bend (C_W/B) was fixed at 0.6. The depth ratio h_r (= h_W/h) between the water head above the overflow crest to the mean depth in the bend was tested by varying the overflow crest level. A total of 18 test runs were carried out for this curved /overflow configuration; 13 runs for

Table 1. Flow Conditions for Combined Curved Channel and Side Overflow Configuration

Test Run	h (mm)	Q (m^3/s)	u_{ms} (m/s)	B/h	h/r_m	C_h (mm)	h_r	Q_r
(1)	(2)	(3)	(4)	(5)	(6)	(7)	(8)	(9)
A1 - A1	55.5	5.38	0.196	9.01	0.037	25	0.55	0.42
A2 - A2	70.0	7.70	0.220	7.14	0.047	25	0.64	0.53
A3 - A3	60.0	6.00	0.200	8.33	0.040	45	0.25	0.13
A4 - A4	70.0	7.39	0.211	7.14	0.047	45	0.36	0.23
A5 - A5	80.0	6.40	0.160	6.25	0.053	65	0.19	0.10

measuring water surface profiles and 5 runs for point velocity and shear stress profiles. In these runs, the tested range of the discharge ratio Q_r (=Q_{cc}/Q) between the side overflow and bend flow was $0.10 < Q_r < 0.75$, and was $0.19 < h_r < 0.71$ for the depth ratio. The detailed analysis of water surface profiles is reported in Fares et al. (1992) and Fares and Herbertson (1993). Attention is given in this study to the comparisons between predicted velocity and shear stress distributions. Table 1 gives the flow conditions for measurements in the curved channel at the lateral overflow intersection. Two cases will be discussed: curved flow with low side overflow ($h_r < 0.36$); and curved flow with high side overflow ($h_r > 0.36$). It should be mentioned that the distributions of depth-averaged velocities $u_m\,(r, s)$ and boundary shear stresses $\tau_0(r, s)$ are normalized by their corresponding values u_{ms} and τ_{0s} respectively, at the upstream reach of the curved channel.

Depth-averaged velocities

Figures 5 and 6 give the longitudinal profiles of the depth-averaged velocities in the curved channel for test runs A3-V3 and A1-V1, which correspond to cases of low and high side overflows respectively. In both figures, the profiles are plotted for bend radii r/r_m = 0.9, 1.0, 1.1 in order to correspond to locations near the inner bank, at the centerline and near the outer bank respectively. As

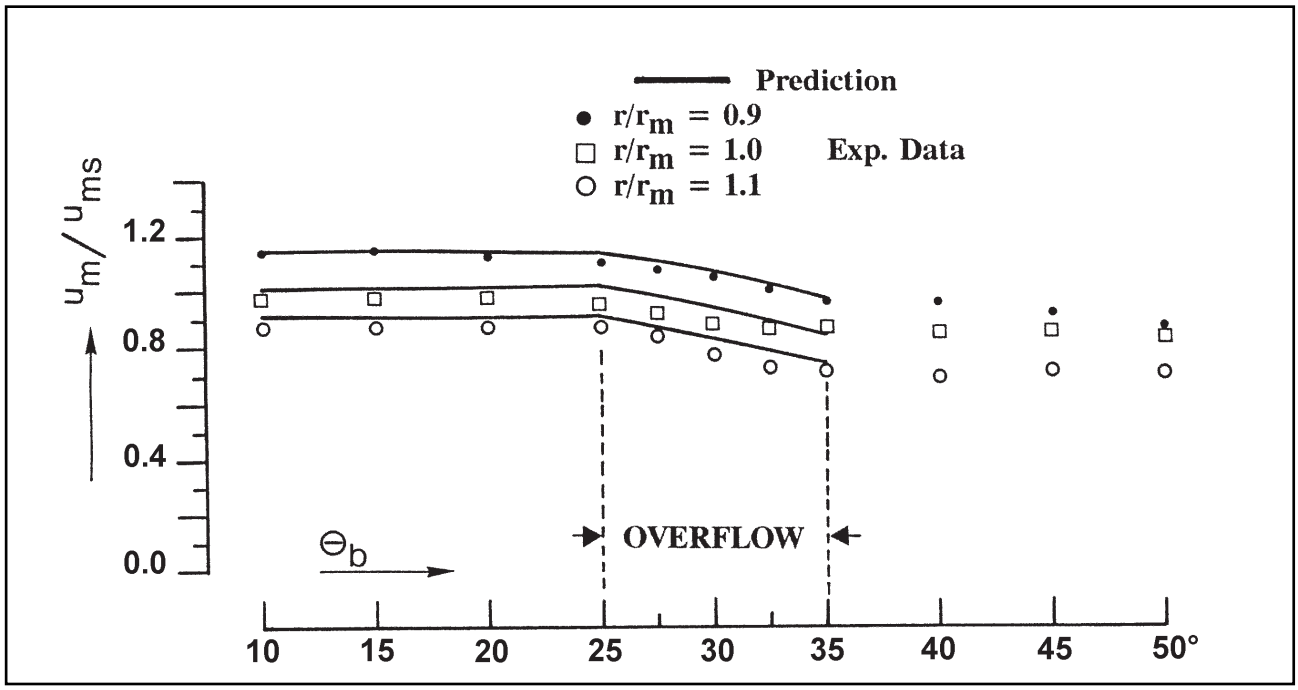

Figure 5. Depth-averaged velocities for low lateral overflow case, test run A3-V3.

can be seen in the figures, for both low and high h_r ratios, a continual reduction in velocities has occurred at the overflow region in the curved channel, particularly in the region close to the overflow ($r/r_m = 1.1$). In addition, higher velocities continue to occupy the inner side of the bend ($r/r_m = 0.9$). This can be explained as follows; as a result of the lateral overflow, the outward cross currents combined with the preexisting secondary flow in the curved channel enhance the outward shifting of momentum and diminish the superelevation at water surface (Fares et al., 1992, Fares, 1995). This process increases across the channel width towards the overflow and results in advection of momentum into the overflow. For the high lateral overflow situation ($h_r > 0.36$), Figure 6, a nearly

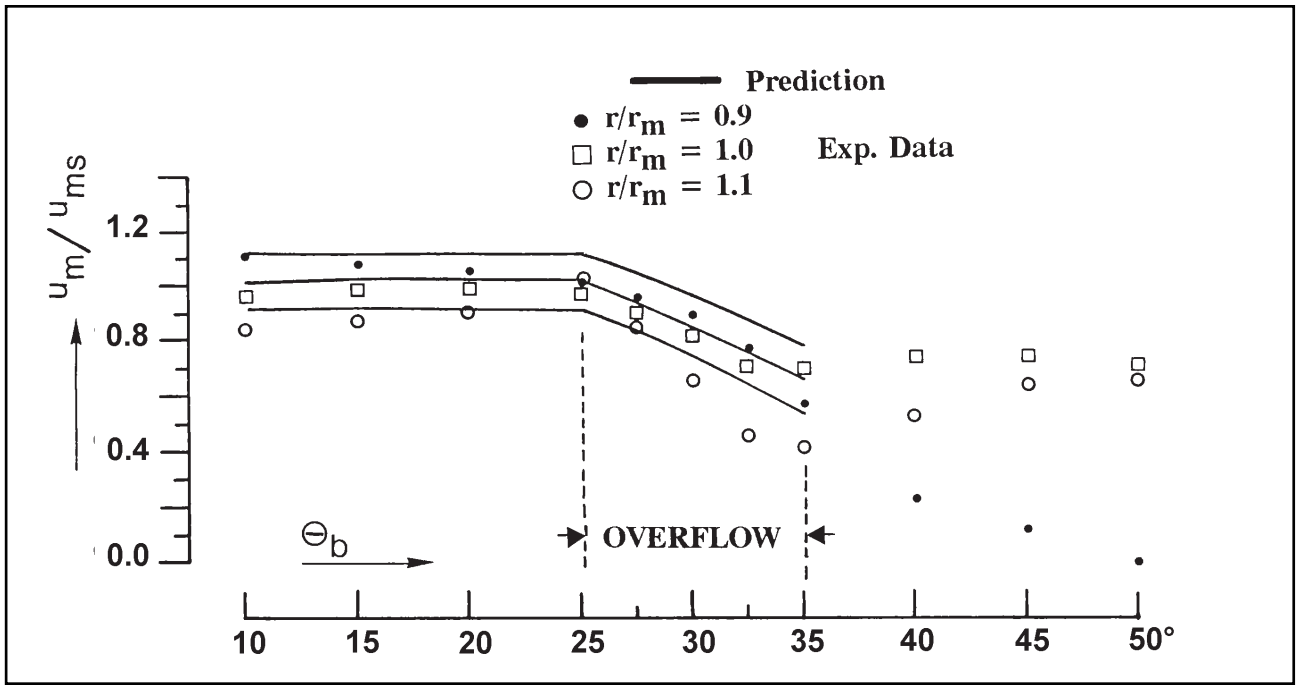

Figure 6. Depth-averaged velocities for high lateral overflow case, test run A1-V1.

uniform distribution across the channel upstream of the overflow is observed. This is attributed to the rapid flow acceleration in the vicinity of the overflow, which increases the transformation of potential energy (depth) into kinetic energy (velocity). Along the intersection, noticeable reduction in velocities was found as a result of the strong outward shift of momentum towards the overflow. In natural streams, the ensuing reduction in velocities in the inner side of the channel would result in the formation of a stagnation zone along the inner bank opposite to the overflow (Jansen et al., 1979).

The comparisons between computed and observed percent reduction in depth-averaged velocities are given in Figure 7. For all h_r ratios, maximum reduction has occurred at the outer side of the channel. For low ratios, the reduction of velocities at the outer side was 18 percent (observed) and 17 percent (predicted), and was 10 percent (observed) and 14 percent (predicted) at the inner side of the channel. For high h_r ratios, the reductions are much higher. For the outer side of the channel, it was 58 percent (observed) and 37 percent (predicted), and for inner side it was 43 percent (observed) and 30 percent (predicted).

Boundary shear stresses

The longitudinal profiles of the shear stresses in the curved channel for test runs A3-V3 and A1-V1 are given in Figures 8 and9, for cases of low and high lateral overflows respectively. For the low overflow case (h_r < 0. 36), Figure 8, the shear stresses at the upstream region of the overflow were slightly affected, while at the intersection, gradual reduction in stresses can be noticed in both predicted and measured profiles. High stresses have continued to occupy the inner side of the channel (r/r_m = 0.9). In the downstream region of the overflow, the stresses along the inner side of the channel decrease steadily while those at the central and outer regions remain virtually constant, in a similar fashion to the velocity profiles (Figure 5).

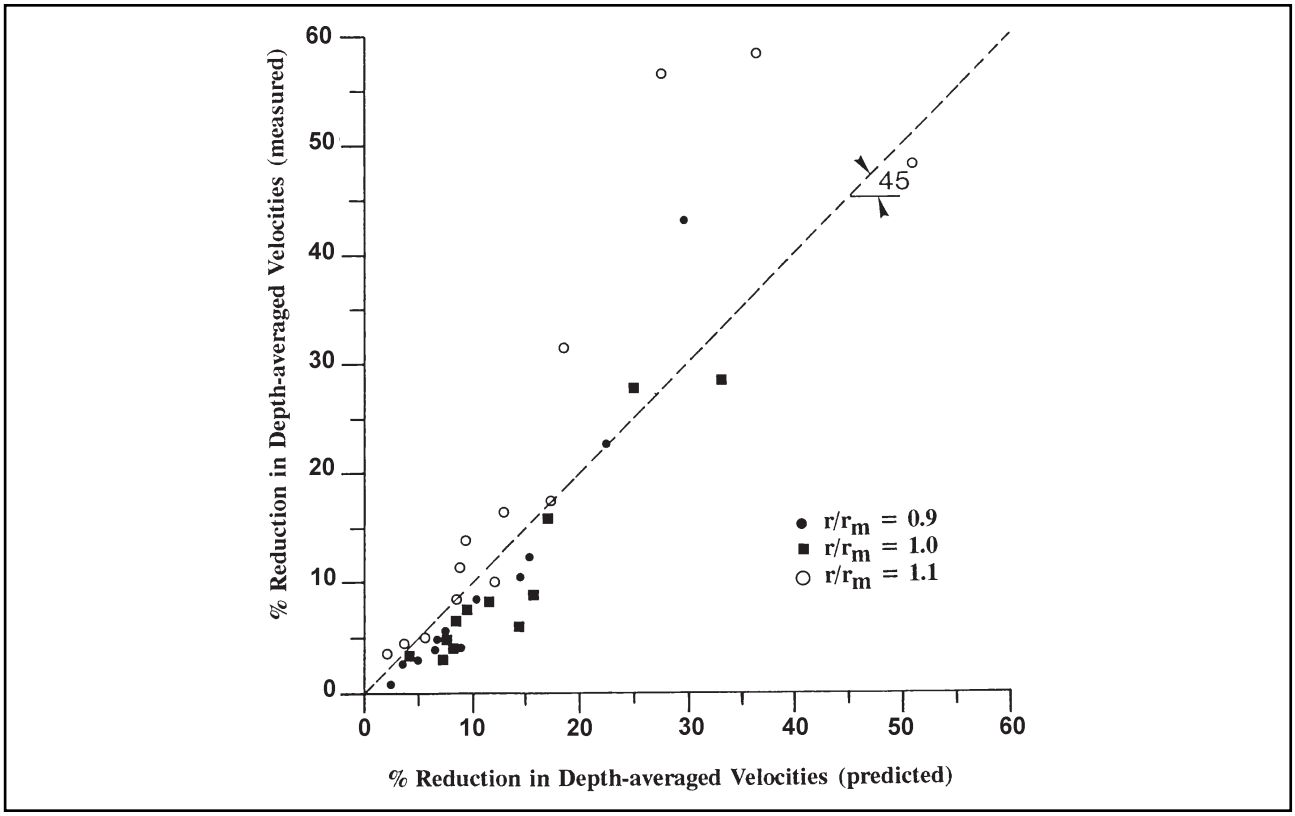

Figure 7. Comparison between predicted and measured reduction in depth-averaged velocities in curved channel at lateral overflow region.

For the case of combined bend and high overflow ($h_r > 0.36$), Figure 9, the stresses at the overflow region are substantially reduced. This is attributed to the strong lateral outward currents, which are responsible for the formation of a sizeable stagnation zone along the inner bank and a separation zone near the outer bank of the channel. Maximum reduction of stresses is always observed at the outer side of the channel. Beyond the overflow intersection, the stresses along the inner channel are reduced as a consequence of the continual growth of the stagnation zone downstream of the overflow region. As a result, high shear stresses become concentrated in the outer half of the channel cross section. Such concentration of stresses indicates that, in a river situation, severe bed scour is likely to occur in this region. This finding has also been experimentally substantiated by observing high velocities of high outward deviations near the channel bed (Fares et al., 1992, Fares and Herbertson, 1993).

The comparisons between predicted and observed percent reduction of shear stresses are shown in Figure 10. For the low overflow case ($h_r < 0.36$), the reduction of shear stresses in the channel was 32 percent (observed) and 37 percent (predicted) at the outer bank, and 19 percent (observed) and

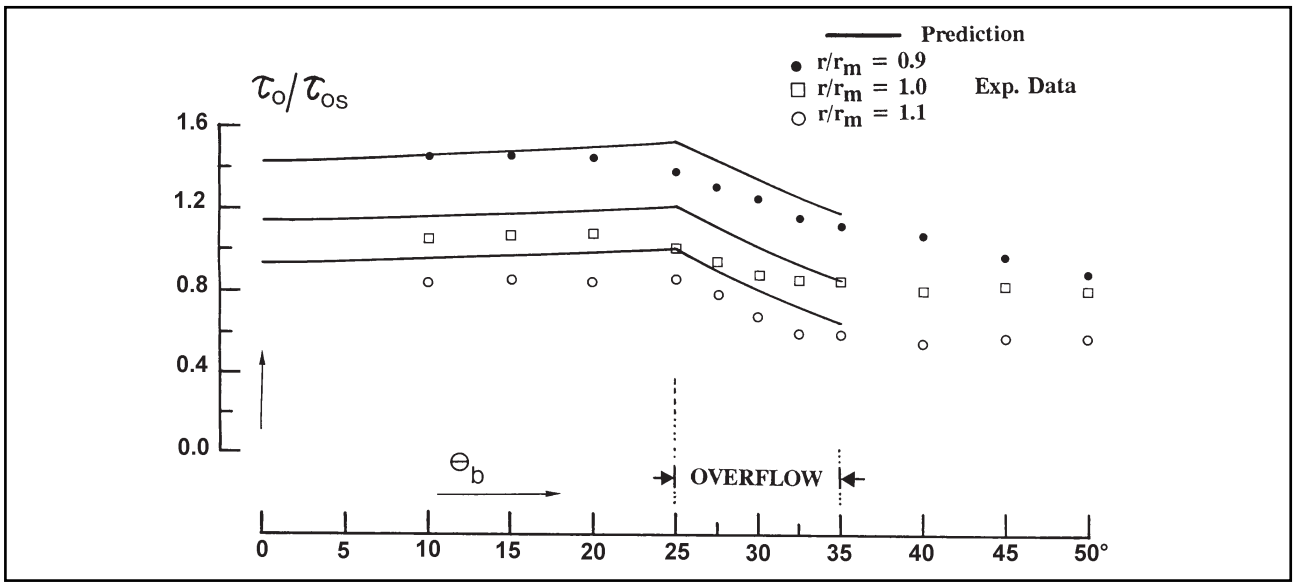

Figure 8. Bed shear stress profiles for low lateral overflow case, test run A3-V3

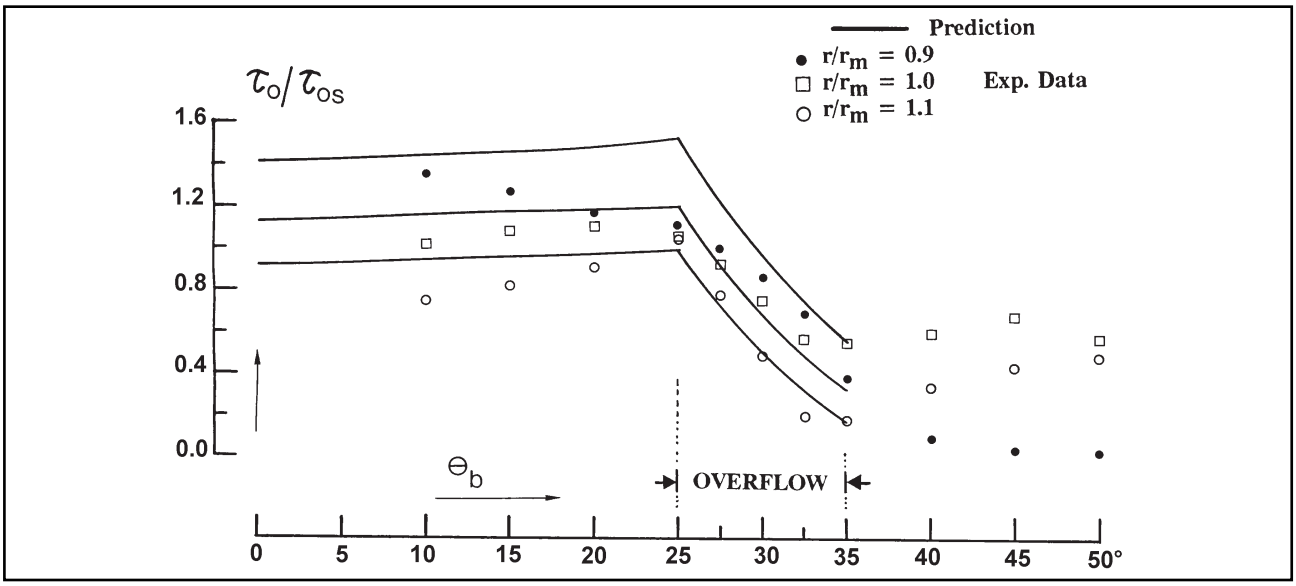

Figure 9. Bed shear stress profiles for high lateral overflow case, test run A1-V1

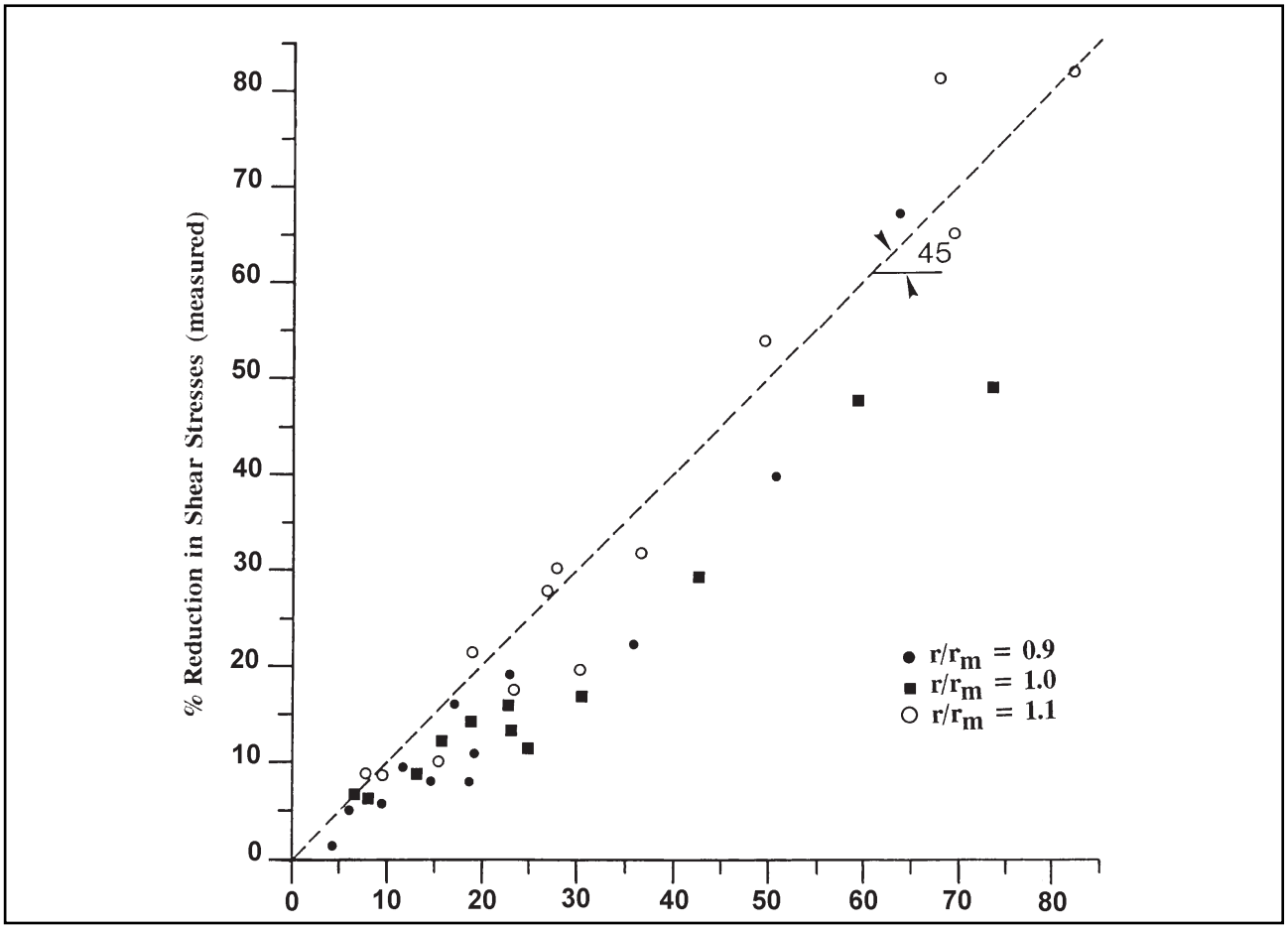

Figure 10. Comparison between predicted and measured reduction in bed shear stresses in curved channel at lateral overflow region.

23 percent (predicted) at the inner bank. For the high overflow case ($h_r > 0.36$), both observed and predicted reduction of stresses was 82 percent at the outer bank, and was 67 percent (observed) and 63 percent (predicted) at the inner bank of the channel.

SUMMARY OF CURVED/LATERAL FLOW MECHANISMS

The computational modeling study presented herein provides an efficient tool for describing the changes occurring to mechanisms of flows in curved channels due to lateral overflows. On the basis of the analysis of velocity and shear stress profiles, the main changes in the curved flow behavior at the lateral overflow intersection can be summarized as follows:

- The principal features of curved flows, i.e. the secondary flow and the superelevation of the water surface, have been significantly altered by the introduction of the lateral overflow. The ensuing changes in velocity and shear stress distributions depend ultimately on the intensity of the overflow (i.e. on h_r and Q_r ratios). In natural streams, these changes will be manifested by the features developed in the bed topography of the river at the intersection region (Figures 1, 2).

- As previously reported in Herbertson and Fares (1991) and Fares and Herbertson (1993), and as implicitly indicated in the analysis of velocity and shear stress profiles, the vertical structure of the secondary flow has been completely transformed, from that typically found in river bends. This again depends on the lateral overflow intensity. For the case of low overflow, the typical "one-cell" type of secondary flow with zero net lateral discharge, has been found to persist but with nonzero lateral discharge due to the surface outward lateral velocities. While in the high overflow case, the vertical

profile of the secondary flow has transformed into a "one-sided" type as the lateral overflow dominated the flow behavior at the intersection.

- For both low and high lateral overflow cases, noticeable reduction in the depth-averaged velocities and boundary shear stress values has occurred. Maximum reduction was always found along the outer side of the curved channel, close to the overflow. For the low overflow situation, a reduction in velocities of up to 18 percent was found at the outer half of the channel. For the high overflow situation, the outer half velocities were reduced by as high as 58 percent. The reduction in shear stresses is more substantial than that in velocities. This is attributed to the increase of water levels, the decrease of velocities and the change of secondary flow cell structure at the overflow region. At the inner bank, the observed reduction in stresses was 19 percent for the low side overflow case, and 67 percent for the high overflow case. While at the outer bank, maximum reduction in stresses was 32 percent for the low overflow situation, and up to 82 percent for the high overflow situation.

- The formation of stagnation and separation zones at the lateral overflow region in the curved channel is found to be a direct result of the changes occurring in flow profiles. The existence of the stagnation zone along the inner bank of the channel has resulted from the strong outward shift of momentum towards the outer bank. This, in turn, has caused considerable reductions in velocities and shear stresses. The formation of stagnation zones has been observed in all flow conditions considered. On the other hand, the formation of the separation zone at the outer half of the channel has resulted from the high concentration of shear stresses which coexists with the continual sizeable growth of the stagnation zone at, and downstream of, the overflow region along the inner bank. Because of this, and of the boundary friction at the outer bank, the separation zone has been formed (see Plates 2 and 3). The effect of the ensuing separation zone in a river situation is the occurrence of severe bed scour along (or close to) the channel outer bank at and downstream of the overflow region, as can be seen in Figures 1 and 2.

BED TOPOGRAPHY IN ALLAN WATER AT CUTOFF SECTION

On the basis of the above analysis of velocity and shear stress profiles carried out on the rigid bed model, an explanation for the bed topography changes in Allan Water at the cutoff section will be attempted. For combined curved and low lateral overflow conditions, the river is expected to be governed by the curved flow regime with an occasional spillage of flood flow across the neck of the cutoff. In contrast, the changes in bed topography are most likely to develop in cases of curved flows combined with high overflows. The occurrence of both longitudinal bar and local scour hole in the bed topography of river (Figures 1 and 2) may be explained qualitatively in terms of velocity (Figures 5 and 6) and shear stress (Figures 8 and 9) distributions obtained from the idealized model study. This can be achieved by matching the locations of features developed in the river situation with those of velocities and shear stresses in the idealized model. By comparing the appropriate locations, a reasonably good correlation between the location of the longitudinal bar and that of minimum velocities and shear stresses along the intersection (at $r/r_m = 1.1$ and $\theta_b = 32.5^o - 35^o$) can be seen. Again by applying the same analogy, the location of the scour hole downstream of the intersection can be detected from the zone of high velocities and shear stresses in the channel at $\theta_b = 40^o - 50^o$ along radii $r/r_m = 1.0$ and 1.1.

Finally, with respect to the migration of the thalweg towards the inside of the curved channel, it was found that both velocities and shear stresses along the inner side of the channel ($r/r_m = 0.9$)

continue to fall rapidly to insignificant values beyond the intersection (Figures 6 and 9, $\theta_b = 40^o - 50^o$). This would indicate that formation of a bar is likely to develop in this region, which would lead eventually to the complete blockage of the meander loop and the development of the oxbow lake

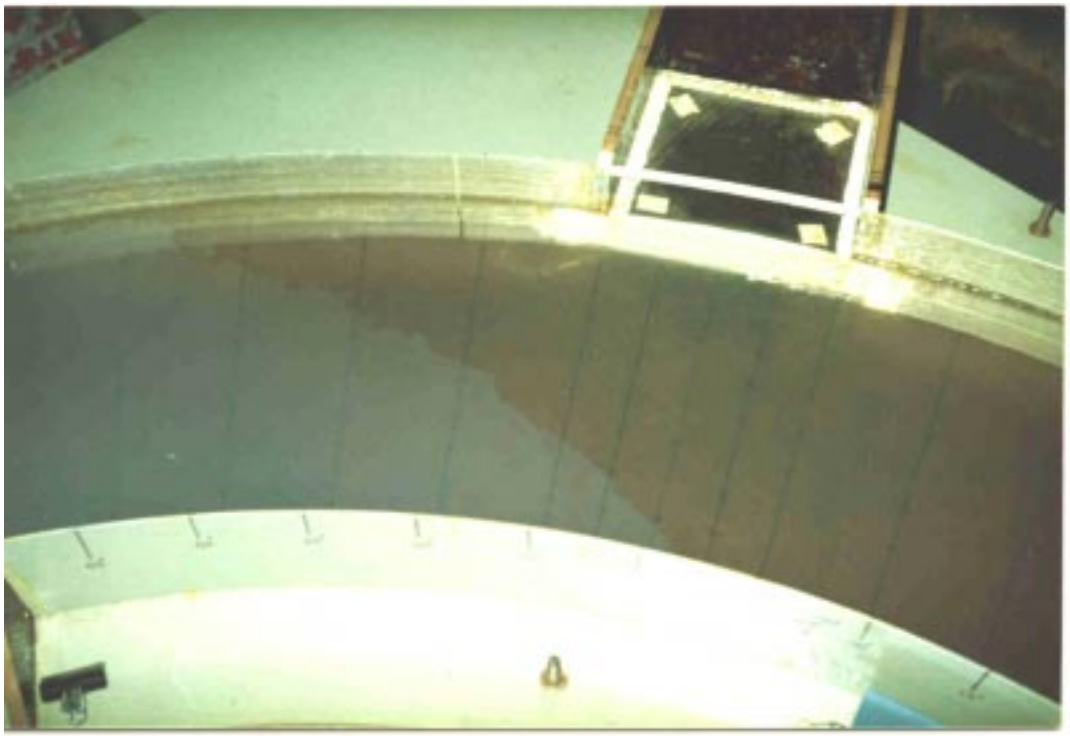

Plate 2. Formation of stagnation zone for low lateral overflow situation, test run A3-V3.

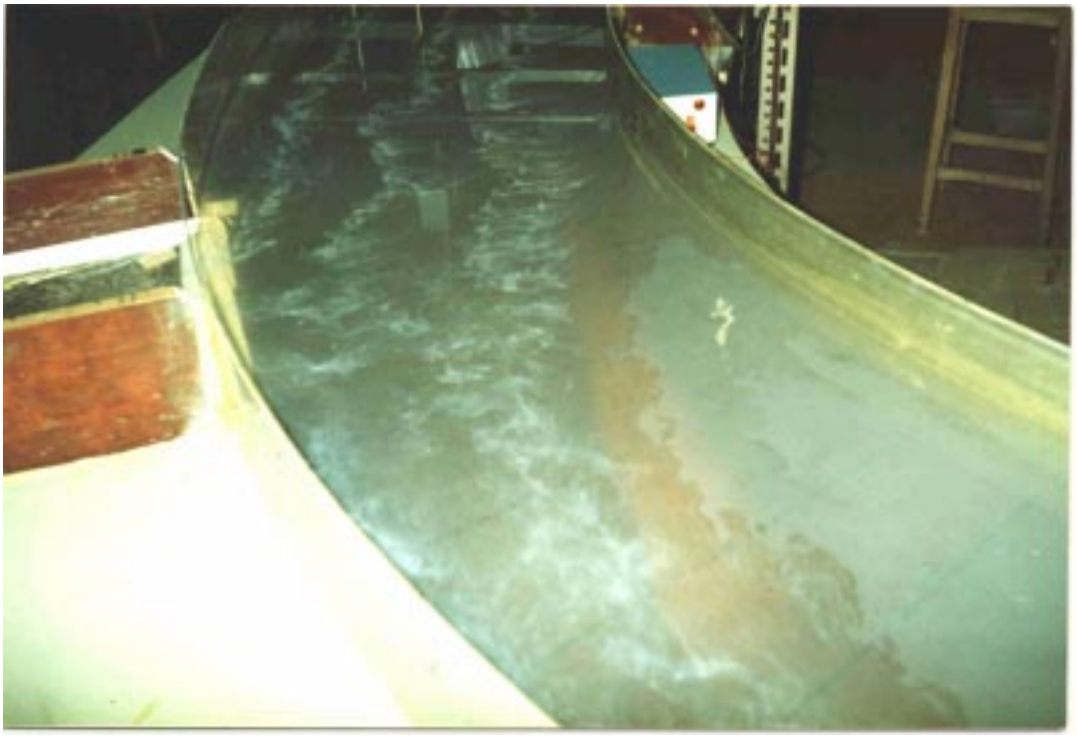

Plate 3. Formation of stagnation zone for high lateral overflow situation, test run A1-V1.

(Allen, 1965). The inward migration of the thalweg has also been observed through the change in the secondary flow cell structure, from the one cell to the two cell type rotating in opposite sense (Figure 2) (Herbertson and Fares, 1991). The change in the cell structure of the secondary flow is initiated by the longitudinal bar development in front of the cutoff (expressed by a zone of minimum shear stresses at $r/r_m = 0.9$ and $\theta_b = 32.5^o - 35^o$, Figure 6). The bar, once it becomes of considerable length, splits the curved flow and, as a consequence, produces the two-cell pattern. This, in turn, forces the flow to move away from the cutoff, thus producing active cutting on the inner side of the channel. It is evident, however, that the existence of zones of high and low stresses in the river at the cutoff section is causing reduction in the river width and hence, encouraging the flow to take the shorter route across the cutoff. Further investigations are recommended into the time and length scales involved in the mechanism by which the meander is adjusted to the cutoff situation in order to provide more rigorous assessment of the long-term stability of the river morphology.

CONCLUSIONS

The characteristic changes occurring to the flow mechanisms in meandering channels at the cutoff intersection were investigated. For the purpose of understanding the mechanisms behind the changes in the bottom topography of the meandering river Allan Water at the cutoff section, a detailed study of velocities and boundary shear stresses in an idealized rigid bed model was undertaken, both computationally and experimentally.

The computational formulation of the problem was developed analytically, and a finite difference method was used to solve the final set of model equations. Key characteristics of curved channel flows (i.e. secondary circulation and superelevation at the water surface) were included in the formulation. The effect of lateral overflow on the river flow was formulated by a spatially varied flow equation with decreasing discharge. The discretized form of the horizontal problem is expressed explicitly and the computational procedure employed in the calculations is described.

It was found from the analysis of results that continual reductions in velocities and shear stresses occurred in the channel at the lateral overflow region. Maximum reductions of velocities and shear stresses were 18 percent and 37 percent respectively for cases of low lateral overflows, and 58 percent and 82 percent respectively for cases of high side overflows respectively. These reductions were attributed to the development of stagnation and separation zones at the intersection associated with strong lateral outward currents.

On the basis of the analysis of the idealized rigid bed model, an explanation for the bed topography changes in Allan Water at the cutoff section was provided. It is found that for the case of combined curved and low lateral overflows, the river is governed by the curved flow regime with an occasional spillage of flood flow across the neck of the cutoff. In contrast, the changes in bed topography are most likely to develop in cases of curved flows combined with high overflows due to the development of stagnation and separation zones at the intersection.

ACKNOWLEDGMENTS

The numerical calculations were carried out using the central HP-UNIX computer service at the University of Surrey, UK. The author wishes to thank Dr J.G. Herbertson of the University of Glasgow for his helpful suggestions throughout the work and for his valuable review of the early draft of the paper.

LIST OF SYMBOLS

A = curved flow area (=$B\,h$)
A_W = weir coefficient includes velocity and discharge coefficients
B = surface channel width
C = Chezy coefficient of boundary roughness
C_h = weir crest height
C_W = across the side overflow can be calculated from
D_f = coefficient for simulating the drowning condition over the weir (# 1)
F_r = Froude number
g = acceleration due to gravity
$h(r,s)$ = local flow depth in the curved channel
h_W = water head above the overflow crest
h_r = ratio between water head above overflow crest and depth in the bend (= h_W/h)
[i,j] = indices for r- and s-directions respectively
[i,l] = indices for r- and s-directions at the overflow region respectively
Q = mean flow discharge in the curved channel
Q_{cc} = lateral overflow (cutoff) discharge
Q_r = the discharge ratio between the side overflow and bend flow (= Q_{cc}/Q)
r = local radius of channel curvature
r_m = mid radius of channel curvature
r, s, z = transverse, longitudinal and vertical cylindrical coordinates respectively
S_0 = river bed slope
S_f = friction (energy) slope
S_S = streamwise flow surface slope
u = sectional velocity of bend flow at the overflow region
$u_m(r,s)$ = local depth-averaged velocity in the curved channel
u_{ms} = mean depth-averaged velocity upstream of the curved channel
u_* = shear (friction) velocity [= $(\tau_S/r)^{1/2}$]
α, β = secondary and main flow convection factors respectively
κ = von-Karman constant
λ = coefficient defined in Equation (9)
$\Phi_1(r,s), \Phi_2(r,s)$ = streamwise and crosswise momentum functions respectively
$\Delta r, \Delta s$ = step size in transverse and longitudinal directions respectively
ΔC_W = step size along s-direction at the overflow region
θ_b = local angle along the curved channel
ρ = flow density
$\tau_0(r,s)$ = the boundary shear stress field [= (τ_r, τ_S)]
τ_{0s} = mean boundary shear stress upstream of the curved channel
(τ_r, τ_S) = transverse and longitudinal shear stress components
$\partial r, \partial s$ = gradient operators in *r*- and *s*-directions respectively

REFERENCES

Allen, J.R.L.; (1965). A review of the origin and characteristics of recent alluvial sediments. Journal of Sedimentology, 5(2), p. 83.

Bouwmeester, J.; (1972). Basic principles for the movement of water in natural and artificial water courses.

Internal Note, Delft University of Technology, Delft, 25 pp.

Chapra, S.C., and R.R. Canale; (1985). Numerical methods for engineers with personal computer applications. 2d edn. McGraw-Hill Book Co., New York, 437 pp.

Chen, G., and H.W. Shen; (1983). River curvature-width ratio effect on shear stress. In: Proceedings of the International Conference on River Meandering ASCE, New Orleans, Louisiana, USA, pp. 687-699.

De Vriend, H.J.; (1981). Velocity redistribution in curved rectangular channels. Fluid Mechanics, 107, pp. 423-439.

Fares, Y.R.; (1994). The CURCLOV - FORTRAN code for calculating the flow mechanisms in rigid bed curved open channels with lateral overflows. Report No. CE/EV0794/01, University of Surrey, UK.

Fares, Y.R.; (1995). Boundary shear in curved channel with side overflow. Journal of Hydraulic Engineering ASCE, 121(1), pp. 2-14.

Fares, Y.R., and J.H. Herbertson; (1993). Behaviour of flow in a channel bend with a side overflow (flood relief) channel. Journal of Hydraulic Research, 31(3), pp. 383-402.

Fares, Y.R., W. Laufs, J. H. Herbertson; (1992). Boundary shear changes in a channel bend at flood relief (cut-off) channel intersection. Report No. CE-FM/FWL/92.1, University of Surrey, UK, 86 pp.

Gagliano, S.M., and P.C. Howard; (1983). The neck cut-off oxbow lake cycle along the lower Mississippi river. Proceedings of the International Conference on River Meandering ASCE, New Orleans, Louisiana, USA, pp. 147-158.

Herbertson, J.G., and Y.R. Fares; (1991). Bed topography changes produced by partial cut-off of a meander loop. Proceedings of the International Conference on Advances in Water Resources Technology, Athens, Greece, pp. 113-120.

Jansen, P.Ph., L. van Bendegom, J. van den Berg, M. de Vries, A. Zanen; (1979). Principles of river engineering, the non-tidal alluvial river. 1st edn. Pitman Pub. Ltd., London, 509 pp.

Johannesson, H., and G. Parker; (1989). Secondary flow in mildly sinuous channel. Journal of Hydraulic Engineering ASCE, 115(3), pp. 289-308.

Kalkwijk, J.P.TH., H.J. De Vriend; (1980). Computation of the flow in shallow river bends. Journal of Hydraulic Research, 18(4), pp. 327-342.

Klaassen, G.T., and B.H.J. van Zanten; (1989). On cut-off ratios of curved channels. Proceedings 23rd Congress of the International Association for Hydraulic Research, Ottawa, Canada, pp. B/121 - B/130.

Price, R.K.; (1977). A mathematical model for river flow - theoretical development. Report No. INT 127, Hydraulic Research Wallingford Ltd., Oxfordshire, UK, 75 pp.

Ranga Raju, K.G., B. Prasad, S.K. Gupta; (1979). Side weir in rectangular channel. Journal of Hydraulics Division ASCE, 105(HY5), pp. 547-554.

Siegenthaler, M.C., and H.W. Shen; (1983). Shear stress uncertainties in bends from equation. Proceedings of the International Conference on River Meandering ASCE, New Orleans, Louisiana, USA, pp. 662-674.

Uyumaz, A., and Y. Muslu; (1985). Flow over side weirs in circular channels. Journal of Hydraulic Engineering ASCE, 111(1), pp. 144-160.

Zimmermann, C., and J.F. Kennedy; (1978). Transverse bed slopes in curved alluvial streams. Journal of Hydraulics Division ASCE, 104(HY1), pp. 33-48.

ADDRESS FOR CORRESPONDENCE
Y.R. Fares
Department of Civil Engineering
University of Surrey
Guildford GU2 7XH
Surrey, U.K.

Email: y.r.fares@the-vine.freeserve.co.uk